



1 An Evaluation of the Performance of Sea-Bird Scientific's Autonomous SeaFET™: 2 Considerations for the Broader Oceanographic Community

3
4 Cale A. Miller^{1,3}, Katie Pocock², Wiley Evans², and Amanda L. Kelley^{1*}

5
6 1. College of Fisheries and Ocean Sciences, University of Alaska Fairbanks, Fairbanks, AK,
7 USA

8
9 2. Hakai Institute, Heriot Bay, BC, Canada

10
11 3. **Present address:** Department of Evolution and Ecology, College of Biological Sciences,
12 University of California Davis, CA, USA

13
14 *Correspondence to: Amanda L. Kelley (alkelley@alaska.edu)

15 16 17 Abstract

18
19 The commercially available Sea-Bird SeaFET™ provides an accessible way for a broad
20 community of researchers to study ocean acidification and obtain robust measurements of
21 seawater pH via the use of an *in situ* autonomous sensor. There are pitfalls, however, that have
22 been detailed in previous best practices for sensor care, deployment, and data handling. Here, we
23 took advantage of two distinctly different coastal settings to evaluate the Sea-Bird SeaFET™ and
24 examine the multitude of scenarios in which problems may arise confounding the accuracy of
25 measured pH. High-resolution temporal measurements of pH were obtained during 3- to 5-month
26 field deployments in three separate locations (two in south-central, Alaska, USA, and one British
27 Columbia, Canada) spanning a broad range of nearshore temperature and salinity conditions.
28 Both the internal and external electrodes onboard the SeaFET™ were evaluated against robust
29 benchtop measurements for accuracy utilizing either the factory calibration, an *in situ* single-
30 point calibration, or *in situ* multi-point calibration. In addition, two sensors deployed in parallel
31 in Kasitsna Bay, AK, USA, were compared for inter-sensor variability in order to quantify other
32 factors contributing to SeaFET™ intrinsic inaccuracies. Based on our results, the multi-point
33 calibration method provided the highest accuracy (< 0.025 difference in pH) of pH when
34 compared against benchtop measurements. Spectral analysis of time series data showed that
35 during spring in Alaskan waters, a range of tidal frequencies dominated pH variability, while
36 seasonal oceanographic conditions were the dominant driver in Canadian waters. Further, it is
37 suggested that spectral analysis performed on initial deployments may be able to act as an *a*
38 *posteriori* method to better identify appropriate calibration regimes. Based on this evaluation, we
39 provide a comprehensive assessment of the potential sources of uncertainty associated with
40 accuracy and precision of the SeaFETs™ electrodes.

41 42 1 Introduction

43
44 The intrusion of excess anthropogenic CO₂ into the global oceans—referred to as ocean
45 acidification (OA)—induces a series of geochemical reactions that increases seawater [H⁺]
46 (lowering pH) while concomitantly reducing the ocean's overall buffering capacity by reducing



the $[\text{CO}_3^{2-}]$ (Caldeira and Wickett, 2003; Orr et al., 2005). Due to more dynamic natural physical and chemical processes in the coastal ocean, a differentiation exists between open-ocean acidification and nearshore coastal acidification. Open-ocean acidification of surface waters is predominately a function of equilibration with atmospheric $p\text{CO}_2$, thus increasing on yearly and decadal timescales as continued burning of fossil fuels ensues (Hofmann et al., 2011; Orr et al., 2005). Coastal acidification, however, can manifest on short time and space scales driven by riverine input and its chemical constituents (e.g., organic carbon, nutrients, and organic alkalinity), community metabolism and organization, tidal cycles, upwelling, and groundwater input (Duarte et al., 2013; Sunda and Cai, 2012; Waldbusser and Salisbury, 2014), all of which can act in conjunction with increasing atmospheric CO_2 , leading to more frequent, intense, and longer-lasting acidification events (Hales et al., 2016; Harris et al., 2013). In the face of rapidly changing coastal conditions, tracking and quantifying the progression of OA requires precise and accurate measurements of carbonate chemistry over long periods of time; these can be achieved by appropriately constraining the carbonate system by measuring at least two of the system's parameters: total dissolved inorganic carbon (TCO_2), total alkalinity (TA), pH, and the partial pressure of CO_2 ($p\text{CO}_2$). Despite the marked increase in OA research over the past decade (Riebesell and Gattuso, 2015; Rudd, 2017), nearshore monitoring efforts—particularly in estuarine waters—have been slow to ramp up, however, efforts are beginning to intensify as technological advancements are made (Feely et al., 2010, 2016; Hales et al., 2016; Harris et al., 2013; Newton et al., 2012; Waldbusser and Salisbury, 2014; Chan et al., 2017).

Acidification of Alaskan coastal waters is predicted to progress rapidly relative to other regions within the next 50 years, and negatively impact the social-ecological structure of Alaskan marine resources by disrupting the Alaska Native subsistence and commercial fisheries (Ekstrom et al., 2015; Mathis et al., 2015b). The ocean waters present along the Alaskan coastline experience chemical and physical drivers of seawater chemistry that are unique to this region. The low seawater temperatures inherently have higher concentrations of dissolved CO_2 , and chemical and physical oceanic processes unique to Alaskan waters such as sea ice melt, glacial discharge, and benthic pelagic coupling across shallow shelves are likely to exacerbate acidification in this region (Evans et al., 2014; Mathis et al., 2011a, 2011b, 2012). Recently, an OA monitoring initiative has been setup by the Alaska Ocean Observing Network (AOOS) to track and provide accessible material dedicated to acidification research in Alaskan waters (<http://www.aos.org/alaska-ocean-acidification-network>). Along the Pacific coast of Alaska, a robust benchtop system known as a Burke-o-Lator (BoL), which measures TCO_2 and $p\text{CO}_2$ either continuously in a flow-through environment or from discrete seawater samples (Bandstra et al., 2006; Barton et al., 2012; Hales et al., 2016) has been installed in several locations, including the OceansAlaska Shellfish Hatchery in Ketchikan, the Alutiiq Pride Shellfish Hatchery in Seward (Evans et al., 2015), and at the Sitka Tribe of Alaska Environmental Research Center (real-time data from Alaskan and other BoLs: http://www.ipacoa.org/Explorer?action=oiw:fixed_platform). Nominal analytical uncertainty for TCO_2 determinations from this system is 0.2% based on the reproducibility of sample and certified reference material (CRM; provided by A. Dickson analyses). For $p\text{CO}_2$ determinations, analytical uncertainty is 1.5% based on the inaccuracy of calculated CRM alkalinity relative to the certified value. While the BoL has significant advantages for achieving robust OA measurements in nearshore waters, the physical constraints of a benchtop system limit the spatial dimension of which carbonate chemistry parameters can be measured. One potential resolution



to diminish the gap in coverage of OA monitoring is to utilize autonomous pH sensors, which are far more versatile in their ability to monitor hard-to-reach areas.

Recent assessments regarding OA monitoring efforts have specifically highlighted the benefits of accessibility by the commercially produced SeaFETTM pH sensor utilizing Honeywell Durafet technology (Martz et al., 2015). The SeaFETTM was originally developed at the Monterey Bay Aquarium Research Institute (Martz et al., 2010), but since has been manufactured and distributed by Satlantic (<http://www.satlantic.com>), which is now incorporated into Sea-Bird Scientific (<http://www.seabird.com>). The partnership between MBARI, Scripps Institute of Oceanography, and Satlantic led the way for commercial availability of the SeaFETTM, providing a ready-to-deploy-factory calibration, quick start manual, and user-friendly interface. The first generation of SeaFETsTM (not distributed by Sea-Bird, but by Dr. Todd Martz at Scripps Institute of Oceanography) have been deployed in numerous field studies and were heavily scrutinized in order to provide robust best practices for appropriate calibration and deployment procedures (Bresnahan et al., 2014; Hofmann et al., 2011; Kapsenberg and Hofmann, 2016; Martz et al., 2010; Matson et al., 2011; Yu et al., 2011). More recent studies have expanded the scope of SeaFETTM accuracy, inter-sensor variability, operator experience, and multi-point calibration techniques (Gonski et al., 2018; Johnson et al., 2017; Kapsenberg et al., 2017; McLaughlin et al., 2017). Given the multitude of information regarding SeaFETTM performance, coalescing all the potential sources of uncertainty in measurements (e.g., inter-sensor variability and calibration method) can be logistically challenging for non-experienced oceanographers who now have access to the commercially available SeaFETsTM distributed by Sea-Bird.

In this study, we aimed to take advantage of two distinct coastal settings in order to deploy and evaluate the commercially available Sea-Bird SeaFETTM, and the potential uncertainties that can arise with time series pH_t (total scale) measurements. For this evaluation, SeaFETsTM were co-deployed side-by-side to quantify inter-sensor variability, discrepancies were examined between factory calibration, *in situ* single-point calibration, and *in situ* multi-point calibration pH_t values, and anomalous data associated with SeaFETTM conditioning times were detailed and considered as potential sources of measurement inaccuracies. All evaluations of SeaFETTM performance were under non-controlled source water conditions or by *in situ* deployments. Three SeaFETsTM were deployed in coastal waters and were subjected to tidal influences and freshwater input, while a fourth was compared to pH_t values derived from measurements obtained by a BoL. Finally, a spectral analysis of the quality-controlled data was performed in order to identify the driving mechanism of pH_t variability between these divergent sites and consider possible un-accounted for calibration errors that could occur in dynamic settings that might not be resolved using a specific calibration method.

2 Methods

2.1 Apparatus: SeaFETTM

The commercially available Sea-Bird SeaFETTM has retained the basic design of the original SeaFETTM developed at MBARI (Martz et al., 2010). The SeaFETTM utilizes the ion sensitive field effect transistor (ISFET) technology, and is outfitted with an internal Honeywell Durafet



and an external solid-state chloride selective electrode (Cl-ISE) along with an internal thermistor, which derives temperature using the (Steinhart and Hart, 1968) equation. The internal reference electrode is intrinsically insensitive to salinity over a tested range from 30 – 36 (Bresnahan et al., 2014), with recent work even suggesting near-ideal Nernstian response to salinity as low as ~9.0 (Gonski et al., 2018). This is in converse to the chloride sensitive external electrode, which is salinity dependent. Both electrodes demonstrate exceptional stability over a range of moderate salinity (30 – 36) and broad temperature (-1 to 35 °C) (Bresnahan et al., 2014; Kapsenberg et al., 2015; Martz et al., 2014, 2010). The range of salinity sensitivity for the external electrode has even been extended down to 20, where it displays a near-ideal Nernst slope (Takeshita et al., 2014). Sea-Bird suggests that the external reference electrode provides the more accurate and stable pH_t measurement given that chloride concentration can be precisely determined from accurate salinity measurements. This is in agreement with previous research demonstrating that the external electrode has a more robust stability (Martz et al., 2010). In dynamic nearshore environments (e.g., estuaries with strong tidal and riverine fluxes), however, the pH_t derived from the internal electrode is recommended (Sea-Bird Scientific's Branham, C., pers. comm.) despite the potential of thermodynamic hysteresis (Martz et al., 2010). Bresnahan et al. (2014) demonstrated that the internal electrode is of the highest quality and under most scenarios remains nearly as stable as the external electrode—this was further corroborated by Gonski et al. (2018) with SeapHOx deployments in the Murderkill estuary, Delaware.

2.2 Calibration

Currently, three different calibration methods are present for the SeaFETTM: a factory pre-deployment single-point calibration, *in situ* single-point calibration, and an *in situ* multi-point calibration (Bresnahan et al., 2014; Gonski et al., 2018). To properly calculate pH_t from SeaFETTM voltage readings, an appropriate calibration coefficient is required. The applied calibration coefficients from the factory are a single-point, pre-deployment calibration. Given that a conditioning period is required for the SeaFETTM (Bresnahan et al., 2014), these coefficients are likely not adequate once the sensor becomes conditioned to the environment to which it is deployed. For the internal electrode, the new calibration coefficient k_{0i} can be determined as

$$k_{0i} = -S_{Nernst} * pH_t + V_{int} - k_{2i} * T, \quad (1)$$

and k_{0e} for the external electrode

$$k_{0e} = V_{ext} - pH_t + \log\left(1 + \frac{S_t}{K_s}\right) - 2 * \log(\gamma_{HCl}) - \log(Cl_T) * S_{nernst} + k_{2e} * T \quad (2)$$

where V_{FET} is the voltage from the electrode and k_2 is the temperature coefficient (dE^*/dT) applied to all SeaFETsTM (Martz et al., 2010). For detailed definitions of S_{nernst} and the salinity dependent constants γ_{HCl} (HCl activity coefficient), Cl_T (total chloride), S_T (total sulfate), and the HSO_4^- dissociation constant K_s (Dickson et al., 2007; Khoo et al., 1977) in equations 1 and 2, we refer readers to Martz et al. (2010), Bresnahan et al. (2014), and Sea-Bird Scientific SeaFETTM Product Manual 2.0.0. In the literature, SeaFETTM calibration coefficients have been denoted as E_{int}^* and E_{ext}^* (Martz et al. 2010, Bresnahan et al. 2014), however, for the purpose of this



evaluation—which specifically examines commercially available Sea-Bird SeaFETs™—the adoption of k_0 and k_2 is in accordance with the preferred nomenclature from the manufacturer.

Unlike the factory pre-deployment single-point calibration, the *in situ* single-point calibration occurs after the sensor has been deployed in the field. At the operator's discretion, a discrete sample will be collected in direct proximity to the deployed SeaFET™ at the same time that the sensor is actively making a measurement, and then measured for pH_t at *in situ* temperature and salinity. The known pH_t would then be used in the above equations as the “ pH_t ” variable. Similar to the single-point *in situ* calibration, the multi-point calibration derives a series of calibration coefficients over a short period of time that is long enough to capture environment variability such as tidal fluxes, and then a single calibration coefficient is averaged. Both single-point calibration methods—pre-deployment and *in situ*—appear to be suitable for fairly static environmental conditions, whereas the multi-point *in situ* calibration is best suited for dynamic nearshore environments (Bresnahan et al., 2014; Gonski et al., 2018).

2.3 SeaFET™ conditioning: test tank deployments

A series of three separate test tank deployments for three SeaFETs™_{395, 396, 397} were conducted in order to determine the conditioning period for each sensor. Initial sensor deployments took place in October 2016 at the Alutiiq Pride Shellfish Hatchery (APSH) in Seward, Alaska. Sensors were deployed for a duration of 72 hours in a flow-through 60 L tank where seawater taken from a depth of ~75 m in Resurrection Bay was sand-filtered, UV treated, and finally run through a 5 μm mesh. All three sensors were programmed with identical sampling settings (Table 1). The onboard internal thermistor was used to calculate temperature, and measurements of seawater salinity incoming to the hatchery were collected by a Sea-Bird Scientific SBE 45 MicroTSG Thermosalinograph that is paired with the BoL and are available on the Alaska Ocean Observing System (<http://portal.aos.org/real-time-sensors.php#map>). Factory calibration coefficients for the internal (k_{0i} , k_{2i}) and external (k_{0e} , k_{2e}) electrodes were retained when processing raw voltage data.

A second tank deployment for the same three SeaFETs™_{395, 396, 397} were deployed at the University of Alaska, Fairbanks, in the Ocean Acidification Research Center (OARC). Seawater collected from the APSH was delivered to the OARC test tank, ~370 L in a half-filled tank. Seawater in the tank was circulated continuously and covered to aid in the prevention of evaporation and photosynthesis. A co-deployed Sea-Bird SBE 16plusV2 SeaCAT (recently serviced by Sea-Bird) collected temperature and salinity readings every 5 minutes. SeaFETs™_{395, 396, 397} were deployed for a duration of nine days in continuous operation mode which forgoes the ability to set frames per burst; average number of reads was identical between all sensors (Table 1). From 1 – 4 November 2016, duplicate discrete bottle samples were collected in 250 ml glass bottles with screw caps at ~00:00 and 17:00 UTC per day. Bottle samples were preserved with 20 μl of saturated HgCl_2 and processed at a later date for TCO_2 and TA with a VINDTA 3C (Versatile Instrument for the Determination of total inorganic carbon and titration alkalinity). The VINDTA 3C has an uncertainty typically near 0.05% (Mathis et al., 2014, 2015a). Bottle sample pH_t was calculated using CO2SYS with known TCO_2 and TA using the constants provided by (Uppström, 1974) and (Lueker et al., 2000); derived pH_t was then compared against SeaFET™ sensor pH_t to test the accuracy of both internal and external



electrodes, assuming the discrete bottle samples were the “true pH” of the seawater. Upon recovery, all SeaFETsTM_{395, 396, 397} were placed into polled mode and stored with wet caps filled with tris buffer (salinity 34, pH 8.09 at room temperature, 25 °C). Again, the factory calibration coefficients for the internal and external electrodes were retained when raw voltage was processed. Since the SBE 16plusV2 sampled every 5 min, salinity and temperature measured by the SBE at each 5-minute point was repeated for the following 4 minutes in order to calculate continuous minute readings by SeaFETsTM_{395, 396, 397}.

A final test tank deployment of the SeaFETsTM_{395, 396, 397} at OARC was conducted after an assumed adequate conditioning period of nine days (first OARC deployment). All three SeaFETsTM_{395, 396, 397} had been set to polled mode after the end of the previous deployment and, therefore, were sleeping for 83 days until this final seven day deployment. The sampling settings were identical to the first OARC deployment for all three SeaFETsTM_{395, 396, 397} (Table 1). Similar to the previous OARC tank deployment, a co-deployed Sea-Bird SBE 16plusV2 SeaCAT collected temperature and salinity mirroring the SeaFET sampling interval of 3 hrs.

The internal thermistor of each SeaFETTM_{395, 396, 397} was tested for accuracy by comparing its derived *in situ* temperature to that collected by the Sea-Bird SBE 16plusV2 during the test tank deployments. The temperature difference between the internal thermistor and the SBE 16plusV2 was used to calculate the average and maximum discrepancy between the two temperature readings. The temperature discrepancy was then applied to a combination of TA: TCO₂ ratios over a range of salinity (20 – 35) in CO2SYS (constants: Uppström, 1974; Lueker et al., 2000), which produced two different pH_i values. The difference between these two pH_i values were, therefore, concluded to be a result of the temperature discrepancy.

2.4 SeaFETTM performance: field deployments

In late winter 2017—32 days post final tank deployment—SeaFETTM₃₉₇ was deployed at the APSH and the two remaining sensors (SeaFETTM_{395, 396}) in Kasitsna Bay within greater Kachemak Bay, Alaska (Fig. 1). At the APSH (60° 5' 55.59"N, 149° 26' 39.80"W), incoming seawater from Resurrection Bay at a depth of 75 m is split before running through a series of hatchery water filters so that an unfiltered line is run directly to the BoL. The incoming line to the BoL was then split to feed an ~11.5 L conical tank housing the SeaFETTM₃₉₇ fit with the copper bio-fouling guard; tank residence time was ~7.5 min. The SeaFETTM₃₉₇ at this location was deployed on 6 March 2017 with a robust sampling setting (Table 1). Two calibration methods were applied for this SeaFETTM₃₉₇, an *in situ* single-point calibration and an *in situ* multi-point calibration. Both calibrations were performed 50 days after deployment on 25 April 2017 once the BoL had completed service maintenance. The single-point *in situ* calibration was taken during midday tide transition in Resurrection Bay, while the multi-point *in situ* approach used five (sensor sampling 3 h intervals) time points spanning an entire tidal cycle. The single-point *in situ* calibration was used to derive k_{0i} for the internal electrode (eq. 1) and k_{0e} for the external electrode (eq. 2). The multi-point *in situ* calibration followed the same formulations with the difference being the final calibration coefficient calculated was the average of the five independently calculated calibration coefficients. Three final pH_i values for the SeaFETTM₃₉₇ were, therefore, calculated based upon the different calibration coefficients (factory, single-point and multi-point *in situ* calibration) and compared against the pH_i determined from continuous



$p\text{CO}_2$ measurements by the BoL and derived TA (TA-S equation, Evans et al. 2015) using CO2SYS with constants provided by Uppström (1974) and Lueker et al. (2000). pH_t uncertainty from the BoL using this combination of measured and derived parameters is 0.007 units based on propagating the error of the BoL $p\text{CO}_2$ uncertainty reported above with the RMSE ($17 \mu\text{mol kg}^{-1}$) of the regional TA-S relationship (Orr, et al., *in prep*).

Inter-sensor variability was examined between two SeaFETsTM_{395, 396} deployed off the pier at the Kasitsna Bay laboratory in Kachemak Bay ($59^\circ 28' 6.71''\text{N}$, $151^\circ 33' 11.12''\text{W}$) ~ 1.5 m from the bottom: depth at this location fluctuates between $\sim 7.5 - 16.8$ m (Fig. 1). On 18 March 2017—44 days post final tank deployment—SeaFETsTM_{395, 396} were attached to the pier piling directly beside one another on a single mooring frame. Both SeaFETsTM were wrapped with pipe tape to minimize biofouling and fit with their respective copper biofouling guards which had a tributyltin plug attached to the inside of the guard. The sampling settings for both SeaFETsTM_{395, 396} were identical to the one at the APSH (Table 1). Five discrete reference samples were taken in duplicate: one sample on day of deployment (UTC: 3-18-17, 18:00), two samples 1-day post-deployment (UTC: 19 March 2017, 03:00 and 15:00), and two samples 2- and 1-day pre-recovery of the SeaFETsTM_{395, 396} (UTC 3 June 2017, 03:00; 6 June 2017, 03:00). Reference samples were collected within 30 s of the instrument sampling time period via a diver's hand Niskin, measured for temperature and salinity with a YSI 3100 conductivity instrument, stored in 250 ml glass bottles with screw caps, poisoned with 100 μl of saturated HgCl_2 , and secured with teflon tape around the bottleneck threading and Parafilm wrapped on the outside of the cap. Calibration samples were processed for TCO_2 and TA with a VINDTA 3C and pH_t calculated using CO2SYS with the constants provided by Uppström (1974) and Lueker et al. (2000). Salinity measurements collected by the Kachemak Bay National Estuarine Research Reserve data sonde, 10 km SE of the deployed sensors ($59^\circ 26' 26.87''\text{N}$, $151^\circ 43' 15.21''\text{W}$), were used along with the SeaFET'sTM internal thermistor readings to calculate pH_t from the raw voltage data in order to capture representative environmental conditions providing relevance for the pH_t time series in this location. A static salinity of 32 was also used for all calculations of pH_t as an assessment of variability due to salinity measured from a data sonde 10 km away. A total of four different pH_t values for both SeaFETsTM_{395, 396} were calculated based on calibration method (factory pre-deployment single-point calibration and the *in situ* single-point) and conditioning: either conditioned or non-conditioned to the environment. All calculated pH_t values from the SeaFETsTM_{395, 396} were then compared against the remaining discrete reference bottle samples not used for calibration. This was done in order to examine the accuracy and inter-sensor variability difference between conditioned and non-conditioned to the environment electrodes. Because the Kachemak Bay data sonde was located 10 km from the deployed SeaFETsTM_{395, 396}, the measured temperature and salinity from the discrete reference samples were used to determine pH_t for the internal and external electrodes at those specific time points. That is, sensor accuracy for these two SeaFETsTM_{395, 396} was only assessed with accurate temperature and salinity values determined from the discrete bottle samples.

A fourth SeaFETTM₂₆₈ operated by the Hakai Institute was deployed on Environment Canada's Sentry Shoal weather buoy in the Northern Strait of Georgia, BC, Canada: $49^\circ 54' 24.00''\text{N}$, $124^\circ 59' 5.99''\text{W}$ (Fig. 1). The Sentry Shoal mooring site is in a water depth of 15 m and the SeaFETTM₂₆₈ was affixed at a depth of 1 m. A pre-deployment bucket test was conducted for 24 h at a sampling interval of 30 min with an average of 10 samples per frame and 30 frames per



burst from 28 – 29 June 2016. SeaFETTM₂₆₈ was outfitted with a copper housing guard and wrapped with copper tape. Sensor underwent two separate deployments, an initial deployment, and a redeployment (6 July and 27 August 2016) that occurred after the sensor was retrieved for cleaning and maintenance. Two separate calibration samples (taken in triplicate) were taken in accordance with each deployment, and occurred 13 and 7 days after each deployment (19 July and 2 September 2016). For each deployment, SeaFETTM₂₆₈ settings were similar to the others at the APSH and in Kasitsna Bay (Table 1). All calibration samples were taken in triplicate at a depth of 1 m via CTD and Niskin bottle castings and collected in 350 ml amber glass bottles with polyurethane-lined crimp-sealed metal caps and poisoned with 200 µl of saturated HgCl₂, and then processed for TCO₂ and pCO₂ with a BoL at the Hakai Institute's Quadra Island Field Station. The measured values were used to derive pH_i using CO2SYS with the constants provided by (Uppström, 1974) and (Lueker et al., 2000) in order to perform a single-point *in situ* calibration. Uncertainty in pH determinations from BoL pCO₂ and TCO₂ measurements was 0.006 units. After SeaFETTM₂₆₈ deployment and calibration, a total of three, triplicate, reference sample sets were taken and processed for pH_i following the procedure used for calibration samples, then compared against SeaFET pH_i.

2.5 Quantifying pH_i and intrinsic sensor uncertainties

Calculating pH_i from the SeaFET'sTM raw voltage reading is dependent on temperature, salinity and an ideal 100% Nernstian response. The software application SeaFETcom permits the operator to automatically calculate pH_i by assigning the calibration coefficient either written to the sensor's header file or the one provided on the CD-ROM (these should be identical). Determination of final pH_i values from the first test tank deployment at the APSH were calculated by two different operators and two sources for the factory pre-deployment single-point calibration coefficients: header file and CD-ROM disc file. Aside from that exception, all other final pH_i values for the internal and external electrodes were calculated with the Mathworks software MATLAB (V. 2016a) and Microsoft excel (v. 2016) using the following equations for the internal electrode

$$pH_{int} = \frac{V_{FET|INT} - k_{0i} - k_{2i} * T}{S_{Nernst}}, \quad (3)$$

and the external electrode

$$pH_{ext} = \frac{V_{FET|EXT} - k_{0e} - k_{2e} * T}{S_{Nernst}} + \log(Cl_T) + 2 * \log(\gamma_{HCl}) - \log\left(1 + \frac{S_T}{K_s}\right) \quad (4)$$

where V_{FET} is the voltage from the electrode and k₂ is the temperature coefficient (dE^{*}/dT) applied to all SeaFETsTM (Martz et al. 2010). Again, for detailed definitions of S_{Nernst} and the salinity dependent constants γ_{HCl} (HCl activity coefficient), Cl_T (total chloride), S_T (total sulfate), and the HSO₄⁻ dissociation constant K_s (Khoo et al. 1977, Dickson et al. 2007) in equations 3 and 4, we refer readers to Martz et al. (2010), Bresnahan et al. (2014), and Sea-Bird Scientific SeaFETTM Product Manual 2.0.0.

2.5.1 Sensor uncertainty

The overall accuracy (i.e., integrated uncertainties) of every SeaFETTM sensor was evaluated by



quantifying all sources of potential uncertainty when calculating a final pH_t from the SeaFETTM. The pH_t uncertainty introduced by calibration method was calculated as the absolute difference between the “true pH_t ” and the final sensor pH_t derived from either factory calibration, the single-point *in situ* calibration, or multi-point *in situ* calibration. The “true pH_t ” was calculated using CO2SYS dissociation constants by Lueker et al., (2000) and Uppström, (1974) with measured TCO_2 and TA via the VINDTA 3C, TCO_2 and $p\text{CO}_2$ measured by the BoL for discrete samples (e.g., SeaFETTM₂₆₈), and $p\text{CO}_2$ and TA (TA-S equation, Evans et al. 2015) for continuous samples (SeaFETTM₃₉₇). A one-way analysis of variance (ANOVA) and the root mean square error (RMSE) were run and calculated in order to compare the pH_t values from both electrodes on SeaFETTM₃₉₇ across calibration methods against the pH_t values from the BoL. The BoL at the APSH sampled every 5 min which produced 256 comparable sample points with a time alignment disparity that ranged from 0 – 120 s against SeaFETTM₃₉₇. The potential pH_t uncertainty based on the thermistor was calculated by using the absolute difference between the thermistor derived temperature and that measured by the SBE 16plusV2 (T_{diff}) from the OARC test tank deployments and the Kasitsna Bay SeaFETsTM_{395, 396} against the Seldovia data sonde 10 km away. Finally, an average inter-sensor variability uncertainty term was calculated as the difference between the two SeaFETsTM_{395, 396} deployed side-by-side in Kasitsna Bay after a single-point *in situ* calibration was performed. All uncertainty terms were calculated and collated based on our evaluations from the Alaska deployed SeaFETsTM_{395, 396, 397}, while SeaFETTM₂₆₈ deployed at Sentry Shoal was only included when determining the accuracy uncertainty term. Due to the disparity between reference samples for the Kasitsna Bay SeaFETsTM_{395, 396} and Sentry Shoal SeaFETTM₂₆₈ (two discrete reference samples) to that at the ASPH SeaFETTM₃₉₇ (256 reference samples), only the average calculated difference (SeaFETTM pH_t – “true pH_t ”) for each calibration method and electrode was used from the APSH SeaFETTM₃₉₇ and then collated with the other reference points from the Kasitsna Bay and Sentry Shoal SeaFETsTM_{395, 396, 268}.

2.5.2 pH_t time series analysis

Final time series analysis was examined in the time and frequency domain using the Mathworks software MATLAB (V. 2016a). Power spectral density was determined via Welch’s method using the pwelch function in MATLAB. Time series data was resampled and linearly interpolated in order to compensate for the missing data points that occurred when sensors arbitrarily stopped sampling.

394

3 Results

396

3.1 Test tank and field conditions

398

Finalized (i.e., calibrated) pH_t values from the first test tank deployment produced two different values, of which each was dependent on whether the calibration coefficient from the header file or the disc file was selected, the result was a difference of ~0.0011 units for both the internal and external electrodes. Because sensors were stored in tris buffer that lacked the addition of bromide between tank deployments and before field deployments, an environmental conditioning period was required for each of the Alaska SeaFETsTM_{395, 396, 397} once submerged in their respective field sites. Thus, any determination of SeaFETTM pH_t accuracy and conditioning period from



tank deployments were inconclusive and will not be considered henceforth. No SeaFETsTM_{395, 396, 397, 268} displayed signs of biofouling or low battery power upon recovery.

SeaFETTM₃₉₇ deployed in parallel with the BoL at the APSH experienced a tank failure on 8 April 2017 resulting in the sensor's emergence for 24 h. In addition, missing temperature and salinity values resulted in gaps of pH_t measurements over the entire deployment. The BoL experienced flow control issues when initial deployment occurred on 6 March 2017 and was not online until 18 April 2017 but, then, operated nearly consistently until 24 May 2017. All pH_t and temperature comparisons were, therefore, made beginning on 18 April 2017.

Due to the *in situ* environmental conditioning period of the Kasitsna Bay SeaFETsTM_{395, 396, 397}, calibration was performed using the initial reference sample collected on 18 March 2017, 03:00 UTC and again with the reference sample collected on 3 June 2017, 03:00 UTC. Due to high variance between duplicate reference samples (SD: 0.08 pH_t) on 19 March 2017, 15:00 UTC, this reference was discarded and not used for comparison or calibration. The Sentry Shoal SeaFETTM₂₆₈ underwent one maintenance and cleaning procedure, including a battery change, during the ~5-month deployment (Table 1). One calibration sample (19 July 2016) and one reference sample (9 November 2016) were averaged from duplicate rather than triplicate replicates due to large variance from one of the replicate samples. The reference sample taken on 23 August 2016, 17:00 UTC was discarded as temperature and salinity data were missing and SeaFETTM₂₆₈ pH_t could not be calculated. The final reference sample (UTC: 9 November 2016, 17:05) was taken 5 min after SeaFETTM₂₆₈ sampled on 9 November 2016, 17:00 UTC.

3.2 Thermistor response: test tank deployment

The internal thermistor amongst the SeaFETsTM_{395, 396, 397} had a difference of less than 0.2 °C over the entirety of the second and third tank deployments. All thermistor derived temperature values had good alignment with the SBE 16plusV2 temperature, and consistently recorded a slightly higher temperature. The discrepancy between the thermistor temperature and SBE16plusV2 was minimal, and reached a maximum of 0.378 (logged by SeaFETTM₃₉₅) during any time over all tank deployments. The average discrepancy, however, was ~0.21 °C when averaging across all SeaFETsTM_{395, 396, 397} and all times.

3.3 Field performance

SeaFETTM₃₉₇ deployed alongside the BoL appeared stable throughout its entire deployment and tracked the pH_t derived from the BoL well (Fig. 2). Errant spikes were present from both electrodes throughout periods before 18 April 2017, which were a result of plumbing changes that occurred to the APSH incoming seawater. On 10 April 2017 the internal thermistor, BoL temp, and BoL salinity fluctuated by 3 °C and 14, respectively, over a 12 h period. These anomalies were removed from analysis. Salinity remained relatively stable throughout the rest of the deployment and ranged from 30.0 – 32.1. The pH_t uncertainty (SeaFETTM – “true” pH_t) decreased, and the accuracy of the SeaFETTM₃₉₇ internal electrode improved once the *in situ* single-point and multi-point calibrations were performed with a RMSE decreasing from 0.5455 pH_t units under factory calibration, 0.0361 pH_t units for *in situ* single-point calibration and 0.0273 pH_t units for the *in situ* multi-point calibration. The external electrode also improved



accuracy with *in situ* single-point and multi-point calibrations with an RMSE of 0.1077 under factory calibration, 0.0390 for *in situ* single-point calibration and 0.0388 for the *in situ* multi-point calibration (Fig. 2). There was a significant difference in the reduction of the pH_t uncertainty for both the internal and external electrodes when utilizing *in situ* single-point and multi-point calibration coefficients compared to the factory calibration coefficients (Table 2). In addition, there was a significant decrease in the pH_t uncertainty when using the *in situ* multi-point calibration coefficients rather than the *in situ* single-point method for the internal electrode, but not for the external electrode (Table 2). The pH_t uncertainty of the internal electrode decreased from 0.0294 units with an *in situ* single-point calibration to 0.0224 units after an *in situ* multi-point calibration. It should be noted that the time alignment disparity which ranged from 0 – 120 s is not considered a significant source of discrepancy as only 4 sample points out of the 256 comparable points were > 0.03 units (i.e., only 4 comparable points greater than the average pH_t uncertainty found after calibration) between any one 5 min sample taken by the BoL. The internal thermistor of SeaFETTM₃₉₇ tracked the recorded BoL temperature trend fairly (Fig. 3), but had a greater magnitude discrepancy than its test tank deployment (~0.21 °C). On average, the thermistor temperature had an absolute difference of 2.83 °C (SD 0.35) from 18 April 2017 – 6 June 2017, which would result in a pH_t uncertainty of ~0.044 units. SeaFETTM₃₉₇ was not fully submerged in the conical tank leaving the top portion susceptible to air temperature fluctuations which could have affected the thermistor readings.

The SeaFETsTM_{395, 396} in Kasitsna Bay improved their accuracy after an *in situ* single-point calibration was performed (Fig. 4), however, this was only the case when sensors were not conditioned as calibration performed after the conditioning period reduced accuracy (Fig. 5). It should be noted that only the pH_t recorded by both SeaFETsTM_{395, 396} at times of the reference samples had precise salinity and temperature (temperature and salinity recorded with reference sample rather than thermistor derived temperature) measurements as all other measurements were calculated from salinity measured by the data sonde 10 km away, and with temperature derived from the onboard thermistor. The pH_t recorded by the external electrode at a fixed salinity displayed little to no variance relative to pH_t calculated with data sonde salinity (< 0.02 pH_t difference: average whether conditioned or non-conditioned to environment). The average pH_t uncertainty from both SeaFETsTM_{395, 396} reduced by approximately half for the internal electrode when not conditioned to the environment after an *in situ* single-point calibration was performed (0.1072 and 0.1394 to 0.0475 and 0.0741 units, respectively), while the external electrode improved only minimally from 0.0988 and 0.0963 to 0.0610 and 0.0894 units, respectively (Fig. 4). When *in situ* single-point calibration was performed after the SeaFETsTM_{395, 396} were conditioned (i.e., calibrated with reference sample taken on 4 June 2017, 03:00 UTC), the pH_t uncertainty for the internal electrode reduced only minimally from factory calibration: 0.1072 and 0.1394 to 0.0896 and 0.1240 units, respectively (Fig. 5a, b). Conversely, the pH_t error for the external electrode increased from 0.0988 and 0.0963 to 0.1011 and 0.1480, respectively (Fig. 5c, d).

Both SeaFETsTM_{395, 396} displayed low inter-sensor variability for the internal electrode, and high for the external electrode after *in situ* single-point calibration was performed on sensors not conditioned to the environment (Fig. 6, gray circles). The mean anomaly between both SeaFETsTM_{395, 396} internal electrodes was 0.0525 units, whereas the external mean anomaly was 0.145 units. When measurements taken before the sensor was conditioned to the environment



(blue shaded region Fig. 6) were removed from analysis, the mean anomaly changed by < 0.006 units for both electrodes. Inter-sensor variability for both electrodes once conditioned, and after *in situ* single-point calibration, was < 0.05 units: 0.0409 and 0.0461 units for the internal and external electrodes, respectively (Fig. 6, black circles). When measurements recorded before the sensors were conditioned to the environment were removed (blue shaded region Fig. 10), the anomaly decreased further, < 0.015 units for both electrodes.

Thermistor readings on both SeaFETsTM_{395, 396} tracked the temperature at the Seldovia site well, however errant spikes occurred around 18 April 2017 and again around 10 May 2017, and continued till the end of the deployment (Fig. 7). The absolute average difference between the thermistor values and the Seldovia data sonde was 0.281°C (SD 0.295), nearly identical to the difference displayed during the test tank deployments, average 0.21°C .

At Sentry Shoal, temperature and salinity seasonally fluctuated and ranged from $8.71 - 21.8^{\circ}\text{C}$ and $23.4 - 29.4$, respectively. There was no clear distinction in greater accuracy between the internal and external electrodes after *in situ* single-point calibration was performed. While the external electrode did display a lower pH_t average uncertainty, this was based on only two reference points, one of which had a time discrepancy of 5 min (9 November 2016, 17:05 UTC). Only two reference samples were comparable against SeaFETTM₂₆₈ pH_t due to the loss of salinity and temperature data on 23 August 2016, 17:00 UTC. Reference samples on 26 September 2016 and 9 November 2016 were, therefore, compared using the new calibration coefficients determined after redeployment on 27 August 2016. The average pH_t uncertainty was < 0.0115 units for both electrodes (Fig. 8) compared to average pH_t uncertainties of 0.0244 and 0.0560 units for the internal and external electrodes, respectively, if initial calibration coefficients from 19 July 2016 were retained. The low pH_t uncertainty (< 0.0137 units) determined after the *in situ* single-point calibration, however, was still greater than the average pH_t uncertainty under factory calibration: < 0.005 units for both electrodes (Fig 8).

3.4 Spectral analysis

All SeaFETsTM_{395, 396, 397, 268} displayed a mixed semi-diurnal tidal response during all field deployments (Fig. 9). SeaFETsTM_{395, 396} at Kasitsna Bay had a stronger amplitude response at a frequency of two cycles d^{-1} , whereas SeaFETTM₃₉₇ had a greater amplitude at one cycle d^{-1} (Fig. 9a, c, d). All three SeaFETsTM_{395, 396, 397} in Alaskan waters had a strong amplitude signal of 1 cycle every 21 days, with an addition signal of one cycle every three days for SeaFETTM₃₉₇. The amplitude signal for SeaFETTM₃₉₇ shifted depending on source of measurement (BoL, internal or external electrode), however, all measurement sources followed the same frequency pattern (Fig 9a). SeaFETTM₂₆₈ displayed a strong signal at a frequency of zero as well as at one and two cycles d^{-1} (Fig 9a).

3.5 Intrinsic uncertainty and accuracy

Among the calculated potential sources of uncertainty in pH_t , inter-sensor variability (difference between SeaFETsTM pH_t) and sensor accuracy produced the greatest uncertainty discrepancies for the internal and external electrodes under factory calibration (Fig. 10). The pH_t uncertainty (i.e., overall sensor accuracy) for the internal electrode reduced a greater degree than the external



electrode at every ordinal calibration method: factory, *in situ* single-point, to *in situ* multi-point calibration (Fig. 10). This was not the case for the external electrode, however, as the overall pH_t accuracy was greater when factory calibration was used compared to an *in situ* single-point calibration was performed after the sensor was conditioned. The thermistor uncertainty (i.e., uncertainty when calculating pH_t based on the thermistor temperature rather than a more accurate temperature gauge) produced a pH_t uncertainty of 0.0044 units, and was based on the recorded values by SeaFETsTM_{395, 396}. Even though the temperature-derived values from the thermistor of SeaFETsTM_{395, 396} were compared against a data sonde 10 km away, the average T_{diff} values were consistent with the T_{diff} calculated from the test tank deployments (within 0.07°C) and, therefore, provided an adequate resolution to determine a thermistor uncertainty value.

4 Discussion

Obtaining accurate and precise measurements of pH in nearshore coastal waters is crucial for understanding changing trends, dynamics, and current baselines of acidification in these—“susceptible to change”—marine domains. For dynamic nearshore systems, the current standard of OA weather (carbonate chemistry variability on timescales of days to months) accuracy should have an uncertainty no greater than 0.02 pH units according to the Global Ocean Acidification Observing Network (Newton et al. 2015). Previous evaluations of the SeaFETTM sensor package have demonstrated accuracy for both electrodes to be better than 0.02 pH units, with a range between 0.01 – 0.04 units for the internal electrode in more dynamic environments (Bresnahan et al., 2014; Gonski, 2018; Martz et al., 2010). Based on our findings, we observed an accuracy range of 0.009 – 0.148 pH_t units after sensors were conditioned and *in situ* single-point or multi-point calibrations were performed for the internal and external electrodes. This range decreased when SeaFETsTM_{395, 396} from Kasitsna Bay were calibrated with reference samples taken at initial deployment (i.e., non-conditioned to environment). For SeaFETTM₃₉₇, the internal electrode’s accuracy was nearly identical to that of the external electrode after an *in situ* multi-point calibration (Fig. 2), suggesting that the internal electrode can produce a highly precise pH_t measurement comparable to the BoL with an accuracy meeting the standards of the OA weather measurements (Newton et al. 2015). This is not to suggest that the SeaFETTM can replace the BoL, particularly because the BoL can capture multiple carbonate chemistry measurements thereby fully constraining the system and identifying potential decoupling of the carbonate system in estuarine waters (Bandstra et al., 2006; Hales et al., 2016). Nonetheless, the SeaFETTM can provide an accurate measurement of pH_t in nearshore waters when SeaFETTM operation is executed with high precision.

SeaFETsTM_{397, 268} deployed at the APSH and at Sentry Shoal displayed the lowest uncertainty and greatest precision of pH_t measurements (Fig. 2 and 8). In both instances, the SeaFETsTM_{397, 268} were adequately conditioned (i.e., subjected to *in situ* conditions for ~50 days) before calibration was performed. The greater overall accuracy displayed by the SeaFETTM₂₆₈ at Sentry Shoal may be due to the fact that the sensor was exposed to *in situ* conditions for a longer period of time and re-calibrated multiple times to the same environment. Further, calibration and reference sample pH_t was derived from TCO_2 and $p\text{CO}_2$ processed by the BoL at Sentry Shoal and from $p\text{CO}_2$ (also measured by BoL) and the TA-salinity relationship (Evans et al. 2015) at the APSH. It is unclear as to why the sensor accuracy of both Kasitsna Bay SeaFETsTM_{395, 396} was substantially less than the SeaFETsTM_{397, 268} at the APSH or Sentry Shoal. A potential reason



for the low accuracy may be that sensors were calibrated at a reference point that was extreme relative to the time series pH_t signal—that is, calibrated at a time of high variability. In this case, performing an *in situ* multiple-point calibration could have reduced the uncertainty and increased the accuracy. While previous studies have found that collection and preservation of calibration and reference samples can result in a decrease in accuracy depending on operator experience (McLaughlin et al., 2017), the operator in this study was considered to have substantial experience conducting such operations used in this evaluation. In addition, given the increased pH_t variability over a short temporal period—which can be seen at the end of the Kasitsna Bay deployment (Fig. 4 and 5)—and the low discrepancy between duplicate reference samples, the former reasoning (i.e., calibrated to an extreme reference point) is a more reasonable explanation for the reduced accuracy by the Kasitsna Bay SeaFETsTM_{395, 396} than operator experience. We reiterate here that reference sample temperature and salinity were used to calculate SeaFETTM pH_t at the time points in which sensor pH_t and reference sample pH_t were compared, thus salinity was not a confounding factor.

Despite the lower accuracy of the Kasitsna Bay SeaFETsTM_{395, 396}, the two sensors provided a better insight of inter-sensor variability for non-conditioned to the environment and conditioned electrodes. After *in situ* single-point calibration for conditioned sensors, the average inter-sensor variability decreased for the internal electrode by ~80%, and >300% for the external electrode (Fig. 6). The inter-sensor variability reported here was still greater than previous findings (Kapsenberg et al., 2017), however, the comparison made in this study was done in the field compared to controlled laboratory conditions as in Kapsenberg et al. (2017). And while non-homogenized water could lead to anomalies in pH_t measurements by the Kasitsna Bay SeaFETsTM_{395, 396}, it is unlikely that water was consistently non-homogenized over the entirety of a deployment at a distance of < 20 cm (distance between electrodes on each SeaFETTM). Furthermore, due to the dynamic nature of Kachemak Bay, where the tidal exchanges are extreme, averaging 4.73 m, it is unlikely that micro-heterogeneity of seawater is the driving force behind the observed differences in pH_t measurements that were observed between SeaFETsTM_{395, 396}. There was a tradeoff for a decrease in inter-sensor variability, as the *in situ* single-point calibration performed after sensors were conditioned resulted in a decrease in accuracy compared to an *in situ* single-point calibration performed for sensors not conditioned to the environment. It should be noted that we do not consider salinity to be a potential source of uncertainty for inter-sensor variability because the pH_t difference using data sonde salinity compared to a fixed salinity resulted in an anomaly of < 0.005 units.

The Sentry Shoal SeaFETTM₂₆₈ had the lowest average pH_t uncertainty for both electrodes after *in situ* single-point calibration was performed, however, these were still greater than the pH_t uncertainty determined using the factory calibration coefficients. This specific example highlights two possibilities: (1) the role of inter-sensor variability, as this may be a coincidental case given the uncertainty observed when quantifying inter-sensor variability, and (2) the influence of variance within a calibration sample set. For the case of SeaFETTM₂₆₈, the replicate calibration samples collected on 19 July 2016 and 2 September 2016 for the first and second deployments had standard deviations of 0.016 and 0.005 pH_t units, respectively. For instances of generally close agreement between factory and *in situ* calibrated data, the variance in the calibration sample set may contribute to better agreement between factory calibrated sensor pH_t data and average discrete sample pH_t measurements. It should also be noted that pre-deployment



calibration can provide highly accurate measurements by the Honeywell Durafet (internal electrode), however, matching exact conditions to those at the field site are necessary (Johnson et al., 2017), and this was not likely the case for the factory provided calibration coefficients.

The evaluation of SeaFETTM performance presented here corroborates and contrasts with previous studies examining the overall accuracy and precision of pH_t measurements made by these oceanographic instruments. While the accuracy of two SeaFETsTM_{397, 268} fall well within the range determined from previous studies, the accuracy of SeaFETsTM_{395, 396} at Kasitsna Bay lay outside the bounds of what has been report in the primary literature (Bresnahan et al., 2014; Gonski et al., 2018; Johnson et al., 2017; Kapsenberg et al., 2017; Martz et al., 2010). Nevertheless, it is relevant to report the potential uncertainties possible when operating SeaFETsTM as a multitude of factors can influence the overall accuracy (e.g., operator, sample preservation, electrode conditioning, calibration measurements), therefore, the potential uncertainties calculated in this study represent the upper limit of an average uncertainty compiled from four different SeaFETsTM (Fig. 10). The utility of such an analysis provides a confidence in SeaFETTM operation, and highlights all the potential uncertainties that need to be considered when deploying the sensors in the field. For example, we have included a thermistor uncertainty term determined from the test tank and field deployments of the Alaska SeaFETsTM_{395, 396, 397}, even though a suitable solution around this issue would be to apply an offset to the thermistor temperature given it was compared to more robust temperature measurements conducted before field deployment. It should be noted, that in this case, the thermistor uncertainty observed from SeaFETTM₃₉₇ against the BoL was excluded as the lag time between thermistor response and tank residence time likely confounded the comparison. The potential pH_t uncertainties presented here should serve as a guide for SeaFETTM operators in order to better understand the source of an uncertainty and take the necessary steps to improve SeaFETTM measurements. Bresnahan et al. (2014) acknowledged that relying on the SeaFETTM for an accurate pH measurement should be viewed cautiously if additional biogeochemical sensors are not co-deployed to cross-validate the stability and accuracy of the SeaFET'sTM electrodes, therefore, being fully aware of all the potential uncertainties presented here will only further aid SeaFETTM operators.

The time series data provided by the SeaFETTM deployments in this study have expanded the scope of spatial pH_t variability along the North American west coast. The SeaFETsTM_{395, 396} deployed in Kasitsna Bay provide some of the first high temporal resolution measurements of pH_t in this region. During this spring deployment, it appears that semi-diurnal tidal fluctuations are the dominant contributor to pH_t variability with an additional cycle occurring every 21 days coinciding with the seasonal spring and neap tides (Fig. 9). The SeaFETTM₂₆₈ at Sentry Shoal also displays a strong pH_t response to the semi-diurnal mixed tidal cycle. A strong signal is also present at a frequency of zero, and is likely a result of the long, across-season, time series. That is, over the course of the entire deployment which went from summer into late fall, seasonal drivers of pH_t (e.g., decrease in water temperature) confounded repetitive frequency patterns. In addition, Sentry Shoal may have a weaker tidal signature relative to other pH_t modulators that do not follow a cyclical pattern such as water mass intrusion, inconsistent metabolic cycles from the end of summer into the fall season, and a shift to the rainy season.

As an elaboration on the power spectral density analysis, we suggest this form of frequency analysis can be utilized to better understand the system in which a SeaFETTM is



deployed, thus informing the operator as to what the drivers of their system are, and when to calibrate the sensor. It is possible that in a highly dynamic setting, the sensor could re-condition over time periods not resolved in a multi-point calibration sampling scheme, and this could enhance sensor inaccuracies. For example, in Kasitsna Bay, a strong semi-diurnal tide cycle was present, so upon redeployment in this area, if possible, the best calibration approach would be an *in situ* multi-point calibration between the M2 cycle. Alternatively, if the system is not driven by a strong tidal signature (e.g., non-coastal region), an *in situ* single point calibration may be a reasonable approach.

5 Conclusion

The following evaluation of the Sea-Bird SeaFETTM helped elucidate the overall accuracy and highlighted the potential uncertainties and pitfalls of operating and obtaining pH_i measurements by the internal and external electrode pair. We found that the internal electrode provided the more robust measurement in nearshore estuarine waters when an *in situ* multi-point calibration was performed (Fig. 10). The quantified potential pH_i uncertainty is based specifically on our findings, whereas further results may minimize this uncertainty given additional evaluations. However, the results here provide an upper limit of the pH_i uncertainty that may be observed when operating a Sea-Bird SeaFETTM. Further, high temporal resolution pH_i measurements in nearshore Canadian and Alaskan waters provide a better understanding of the drivers modulating pH on short timescales. Given the application, the Sea-Bird SeaFETTM can provide a reliable and accurate pH_i measurement which can be utilized to broaden the coverage of understanding pH variability in nearshore and open-ocean waters.

Acknowledgments

The authors would like to thank Jeff Hetrick and Jacqueline Ramsey at the Alutiiq Pride Shellfish Hatchery for providing their facilities and services for this evaluation. We would also like to thank Angela Doroff at the Kasitsna Bay laboratory for providing facilities for SeaFETTM deployments. Funding for this project was provided in part by the University of Alaska Fairbanks College of Fisheries and Ocean Sciences. WE and KP thank the Pacific Salmon Foundation and Environment Canada for providing the platform for deploying SeaFET 268, the University of Alaska Fairbanks Ocean Acidification Research Center for the long-term use of SeaFET 268, and the Tula Foundation for supporting their efforts with this work.

References

- Bandstra, L., Hales, B. and Takahashi, T.: High-frequency measurements of total CO₂: Method development and first oceanographic observations, *Mar. Chem.*, 100(1–2), 24–38, doi:10.1016/j.marchem.2005.10.009, 2006.
- Barton, A., Hales, B., Waldbusser, G. G., Langdon, C. and Feely, R. A.: The Pacific oyster, *Crassostrea gigas*, shows negative correlation to naturally elevated carbon dioxide levels: Implications for near-term ocean acidification effects, *Limnol. Oceanogr.*, 57(3), 698–710, doi:10.4319/lo.2012.57.3.0698, 2012.



- 725 Bresnahan, P. J., Martz, T. R., Takeshita, Y., Johnson, K. S. and LaShomb, M.: Best practices for
726 autonomous measurement of seawater pH with the Honeywell Durafet, *Methods Oceanogr.*, 9,
727 44–60, doi:10.1016/j.mio.2014.08.003, 2014.
- 728 Caldeira, K. and Wickett, M. E.: Anthropogenic carbon and ocean pH, *Nature*, 425(6956), 365–
729 365, doi:10.1038/425365a, 2003.
- 730 Chan, F., Barth, J. A., Blanchette, C. A., Byrne, R. H., Chavez, F., Cheriton, O., Feely, R. A.,
731 Friederich, G., Gaylord, B., Gouhier, T., Hacker, S., Hill, T., Hofmann, G., McManus, M. A.,
732 Menge, B. A., Nielsen, K. J., Russell, A., Sanford, E., Sevdjian, J. and Washburn, L.: Persistent
733 spatial structuring of coastal ocean acidification in the California Current System, *Sci. Rep.*, 7(1),
734 2526, doi:10.1038/s41598-017-02777-y, 2017.
- 735 Dickson, A. G., Sabine, C. L. and Christian, J. R.: Guide to Best Practices for Ocean CO₂
736 Measurements., Report, North Pacific Marine Science Organization. [online] Available from:
737 <http://www.oceandatapactices.net:80/handle/11329/249>, 2007.
- 738 Duarte, C. M., Hendriks, I. E., Moore, T. S., Olsen, Y. S., Steckbauer, A., Ramajo, L.,
739 Carstensen, J., Trotter, J. A. and McCulloch, M.: Is Ocean Acidification an Open-Ocean
740 Syndrome? Understanding Anthropogenic Impacts on Seawater pH, *Estuaries Coasts*, 36(2),
741 221–236, doi:10.1007/s12237-013-9594-3, 2013.
- 742 Ekstrom, J. A., Suatoni, L., Cooley, S. R., Pendleton, L. H., Waldbusser, G. G., Cinner, J. E.,
743 Ritter, J., Langdon, C., van Hooidonk, R., Gledhill, D., Wellman, K., Beck, M. W., Brander, L.
744 M., Rittschof, D., Doherty, C., Edwards, P. E. T. and Portela, R.: Vulnerability and adaptation of
745 US shellfisheries to ocean acidification, *Nat. Clim. Change*, 5(3), 207–214,
746 doi:10.1038/NCLIMATE2508, 2015.
- 747 Evans, W., Mathis, J. T. and Cross, J. N.: Calcium carbonate corrosivity in an Alaskan inland
748 sea, *Biogeosciences*, 11(2), 365–379, doi:10.5194/bg-11-365-2014, 2014.
- 749 Evans, W., Mathis, J. T., Ramsay, J. and Hetrick, J.: On the Frontline: Tracking Ocean
750 Acidification in an Alaskan Shellfish Hatchery, *PLOS ONE*, 10(7), e0130384,
751 doi:10.1371/journal.pone.0130384, 2015.
- 752 Feely, R. A., Alin, S. R., Newton, J., Sabine, C. L., Warner, M., Devol, A., Krembs, C. and
753 Maloy, C.: The combined effects of ocean acidification, mixing, and respiration on pH and
754 carbonate saturation in an urbanized estuary, *Estuar. Coast. Shelf Sci.*, 88(4), 442–449,
755 doi:10.1016/j.ecss.2010.05.004, 2010.
- 756 Feely, R. A., Alin, S. R., Carter, B., Bednaršek, N., Hales, B., Chan, F., Hill, T. M., Gaylord, B.,
757 Sanford, E., Byrne, R. H., Sabine, C. L., Greeley, D. and Juranek, L.: Chemical and biological
758 impacts of ocean acidification along the west coast of North America, *Estuar. Coast. Shelf Sci.*,
759 183, Part A, 260–270, doi:10.1016/j.ecss.2016.08.043, 2016.
- 760 Gonski, S. F., Cai, W.-J., Ullman, W. J., Joesoef, A., Main, C. R., Pettay, D. T. and Martz, T. R.:
761 Assessment of the suitability of Durafet-based sensors for pH measurement in dynamic estuarine



- 762 environments, *Estuar. Coast. Shelf Sci.*, 200(Supplement C), 152–168,
763 doi:10.1016/j.ecss.2017.10.020, 2018.
- 764 Hales, B., Suhrbier, A., Waldbusser, G. G., Feely, R. A. and Newton, J. A.: The Carbonate
765 Chemistry of the “Fattening Line,” Willapa Bay, 2011–2014, *Estuaries Coasts*, 1–14,
766 doi:10.1007/s12237-016-0136-7, 2016.
- 767 Harris, K. E., DeGrandpre, M. D. and Hales, B.: Aragonite saturation state dynamics in a coastal
768 upwelling zone, *Geophys. Res. Lett.*, 40(11), 2720–2725, doi:10.1002/grl.50460, 2013.
- 769 Hofmann, G. E., Smith, J. E., Johnson, K. S., Send, U., Levin, L. A., Micheli, F., Paytan, A.,
770 Price, N. N., Peterson, B., Takeshita, Y., Matson, P. G., Crook, E. D., Kroeker, K. J., Gambi, M.
771 C., Rivest, E. B., Frieder, C. A., Yu, P. C. and Martz, T. R.: High-Frequency Dynamics of Ocean
772 pH: A Multi-Ecosystem Comparison, *Plos One*, 6(12), e28983,
773 doi:10.1371/journal.pone.0028983, 2011.
- 774 Johnson, K. S., Plant, J. N., Coletti, L. J., Jannasch, H. W., Sakamoto, C. M., Riser, S. C., Swift,
775 D. D., Williams, N. L., Boss, E., Haentjens, N., Talley, L. D. and Sarmiento, J. L.:
776 Biogeochemical sensor performance in the SOCCOM profiling float array, *J. Geophys. Res.-*
777 *Oceans*, 122(8), 6416–6436, doi:10.1002/2017JC012838, 2017.
- 778 Kapsenberg, L., Bockmon, E. E., Bresnahan, P. J., Kroeker, K. J., Gattuso, J.-P. and Martz, T.
779 R.: Advancing Ocean Acidification Biology Using Durafet® pH Electrodes, *Front. Mar. Sci.*, 4,
780 doi:10.3389/fmars.2017.00321, 2017.
- 781 Kapsenberg, L. and Hofmann, G. E.: Ocean pH time-series and drivers of variability along the
782 northern Channel Islands, California, USA, *Limnol. Oceanogr.*, 61(3), 953–968,
783 doi:10.1002/lno.10264, 2016.
- 784 Kapsenberg, L., Kelley, A. L., Shaw, E. C., Martz, T. R. and Hofmann, G. E.: Near-shore
785 Antarctic pH variability has implications for the design of ocean acidification experiments, *Sci.*
786 *Rep.*, 5, srep09638, doi:10.1038/srep09638, 2015.
- 787 Khoo, K. H., Ramette, R. W., Culberson, C. H. and Bates, R. G.: Determination of hydrogen ion
788 concentrations in seawater from 5 to 40.degree.C: standard potentials at salinities from 20 to
789 45%, *Anal. Chem.*, 49(1), 29–34, doi:10.1021/ac50009a016, 1977.
- 790 Lueker, T. J., Dickson, A. G. and Keeling, C. D.: Ocean pCO₂ calculated from dissolved
791 inorganic carbon, alkalinity, and equations for K₁ and K₂: validation based on laboratory
792 measurements of CO₂ in gas and seawater at equilibrium, *Mar. Chem.*, 70(1–3), 105–119,
793 doi:10.1016/S0304-4203(00)00022-0, 2000.
- 794 Martz, T., Send, U., Ohman, M. D., Takeshita, Y., Bresnahan, P., Kim, H.-J. and Nam, S.:
795 Dynamic variability of biogeochemical ratios in the Southern California Current System,
796 *Geophys. Res. Lett.*, 41(7), 2496–2501, doi:10.1002/2014GL059332, 2014.
- 797 Martz, T. R., Connery, J. G. and Johnson, K. S.: Testing the Honeywell Durafet® for seawater
798 pH applications, *Limnol. Oceanogr. Methods*, 8(5), 172–184, doi:10.4319/lom.2010.8.172, 2010.



- 799 Martz, T. R., Daly, K. L., Byrne, R. H., Stillman, J. H. and Turk, D.: Technology for ocean
800 acidification research: needs and availability, *Oceanography*, 28(2), 40–47, 2015.
- 801 Mathis, J. T., Cross, J. N. and Bates, N. R.: Coupling primary production and terrestrial runoff to
802 ocean acidification and carbonate mineral suppression in the eastern Bering Sea, *J. Geophys.*
803 *Res. Oceans*, 116(C2), C02030, doi:10.1029/2010JC006453, 2011a.
- 804 Mathis, J. T., Cross, J. N. and Bates, N. R.: The role of ocean acidification in systemic carbonate
805 mineral suppression in the Bering Sea, *Geophys. Res. Lett.*, 38(19), L19602,
806 doi:10.1029/2011GL048884, 2011b.
- 807 Mathis, J. T., Pickart, R. S., Byrne, R. H., McNeil, C. L., Moore, G. W. K., Juranek, L. W., Liu,
808 X., Ma, J., Easley, R. A., Elliot, M. M., Cross, J. N., Reisdorph, S. C., Bahr, F., Morison, J.,
809 Lichendorf, T. and Feely, R. A.: Storm-induced upwelling of high pCO₂ waters onto the
810 continental shelf of the western Arctic Ocean and implications for carbonate mineral saturation
811 states, *Geophys. Res. Lett.*, 39(7), L07606, doi:10.1029/2012GL051574, 2012.
- 812 Mathis, J. T., Cross, J. N., Monacci, N., Feely, R. A. and Staben, P.: Evidence of prolonged
813 aragonite undersaturations in the bottom waters of the southern Bering Sea shelf from
814 autonomous sensors, *Deep-Sea Res. Part II-Top. Stud. Oceanogr.*, 109, 125–133,
815 doi:10.1016/j.dsr2.2013.07.019, 2014.
- 816 Mathis, J. T., Cross, J. N., Evans, W. and Doney, S. C.: Ocean Acidification in the Surface
817 Waters of the Pacific-Arctic Boundary Regions, *Oceanography*, 28(2), 122–135,
818 doi:10.5670/oceanog.2015.36, 2015a.
- 819 Mathis, J. T., Cooley, S. R., Lucey, N., Colt, S., Ekstrom, J., Hurst, T., Hauri, C., Evans, W.,
820 Cross, J. N. and Feely, R. A.: Ocean acidification risk assessment for Alaska’s fishery sector,
821 *Prog. Oceanogr.*, 136, 71–91, doi:10.1016/j.pocean.2014.07.001, 2015b.
- 822 Matson, P. G., Martz, T. R. and Hofmann, G. E.: High-frequency observations of pH under
823 Antarctic sea ice in the southern Ross Sea, *Antarct. Sci.*, 23(6), 607–613,
824 doi:10.1017/S0954102011000551, 2011.
- 825 McLaughlin, K., Dickson, A., Weisberg, S. B., Coale, K., Elrod, V., Hunter, C., Johnson, K. S.,
826 Kram, S., Kudela, R., Martz, T., Negrey, K., Passow, U., Shaughnessy, F., Smith, J. E., Tadesse,
827 D., Washburn, L. and Weis, K. R.: An evaluation of ISFET sensors for coastal pH monitoring
828 applications, *Reg. Stud. Mar. Sci.*, 12, 11–18, doi:10.1016/j.rsma.2017.02.008, 2017.
- 829 Newton J.A., Feely R. A., Jewett E. B., Williamson P. & Mathis J.
830 2015. Global Ocean Acidification Observing Network: Requirements and Governance Plan.
831 Second Edition, GOA-ON, http://www.goa-on.org/docs/GOA-ON_plan_print.pdf.
832
- 833 Newton, J., Devol, A., Alford, M., Mickett, J., Sabine, C. and Sutton, A.: Nanoos Contributions
834 to Understanding Ocean Acidification, *J. Shellfish Res.*, 31(1), 327–327, 2012.
- 835 Orr, J. C., Fabry, V. J., Aumont, O., Bopp, L., Doney, S. C., Feely, R. A., Gnanadesikan, A.,
836 Gruber, N., Ishida, A., Joos, F., Key, R. M., Lindsay, K., Maier-Reimer, E., Matear, R., Monfray,



- 837 P., Mouchet, A., Najjar, R. G., Plattner, G. K., Rodgers, K. B., Sabine, C. L., Sarmiento, J. L.,
838 Schlitzer, R., Slater, R. D., Totterdell, I. J., Weirig, M. F., Yamanaka, Y. and Yool, A.:
839 Anthropogenic ocean acidification over the twenty-first century and its impact on calcifying
840 organisms, *Nature*, 437(7059), 681–686, doi:10.1038/nature04095, 2005.
- 841 Orr, J. C., J.-M. Epitalon, A. G. Dickson, and J.-P. Gattuso: Routine uncertainty propagation for
842 the marine carbon dioxide system, *Marine Chemistry*, *in prep.*
843
- 844 Riebesell, U. and Gattuso, J.-P.: Lessons learned from ocean acidification research, *Nat. Clim.*
845 *Change*, 5(1), 12–14, doi:10.1038/nclimate2456, 2015.
- 846 Rudd, M. A.: What a Decade (2006–15) Of Journal Abstracts Can Tell Us about Trends in
847 Ocean and Coastal Sustainability Challenges and Solutions, *Front. Mar. Sci.*, 4,
848 doi:10.3389/fmars.2017.00170, 2017.
- 849 Steinhart, J. S. and Hart, S. R.: Calibration curves for thermistors, *Deep Sea Res. Oceanogr.*
850 *Abstr.*, 15(4), 497–503, doi:10.1016/0011-7471(68)90057-0, 1968.
- 851 Sunda, W. G. and Cai, W.-J.: Eutrophication Induced CO₂-Acidification of Subsurface Coastal
852 Waters: Interactive Effects of Temperature, Salinity, and Atmospheric P-CO₂, *Environ. Sci.*
853 *Technol.*, 46(19), 10651–10659, doi:10.1021/es300626f, 2012.
- 854 Takeshita, Y., Martz, T. R., Johnson, K. S. and Dickson, A. G.: Characterization of an Ion
855 Sensitive Field Effect Transistor and Chloride Ion Selective Electrodes for pH Measurements in
856 Seawater, *Anal. Chem.*, 86(22), 11189–11195, doi:10.1021/ac502631z, 2014.
- 857 Upström, L. R.: The boron/chlorinity ratio of deep-sea water from the Pacific Ocean, *Deep Sea*
858 *Res. Oceanogr. Abstr.*, 21, 161–162, doi:10.1016/0011-7471(74)90074-6, 1974.
- 859 Waldbusser, G. G. and Salisbury, J. E.: Ocean Acidification in the Coastal Zone from an
860 Organism's Perspective: Multiple System Parameters, Frequency Domains, and Habitats,
861 *Annu. Rev. Mar. Sci.*, 6(1), 221–247, doi:10.1146/annurev-marine-121211-172238, 2014.
- 862 Yu, P. C., Matson, P. G., Martz, T. R. and Hofmann, G. E.: The ocean acidification seascape and
863 its relationship to the performance of calcifying marine invertebrates: Laboratory experiments on
864 the development of urchin larvae framed by environmentally-relevant pCO₂/pH, *J. Exp. Mar.*
865 *Biol. Ecol.*, 400(1–2), 288–295, doi:10.1016/j.jembe.2011.02.016, 2011.
- 866
867
868
869
870
871
872
873
874
875



Table 1. Deployment regime of all four SeaFETsTM including deployment location, date, and calibration methods performed. *Non-controlled source water pumped directly from Resurrection Bay, AK, USA.

Location (Tank or Field)	Date	SeaFET TM ID	Average reads frame ⁻¹	Frames Burst ⁻¹	Sampling Freq. (min)	Calibration method
APSH — <i>Tank</i>	5 – 8 October 2016	395, 396, 397	1	10	5	Factory
OARC — <i>Tank</i>	26 October – 3 November 2016	395, 396, 397	3	—	Continuous	Factory
OARC — <i>Tank</i>	26 January – 1 February 2017	395, 396, 397	1	10	180	Factory
APSH <i>Field</i> *	5 March – 6 June 2017	397	10	30	180	Factory, SP and MP <i>in situ</i>
Kachemak Bay <i>Field</i>	18 March – 4 June 2017	395, 396	10	30	180	Factory, SP <i>in situ</i>
Sentry Shoal <i>Field</i>	6 July – 23 August, 27 August – 28 November 2016	268	10	30	30	Factory, SP <i>in situ</i>

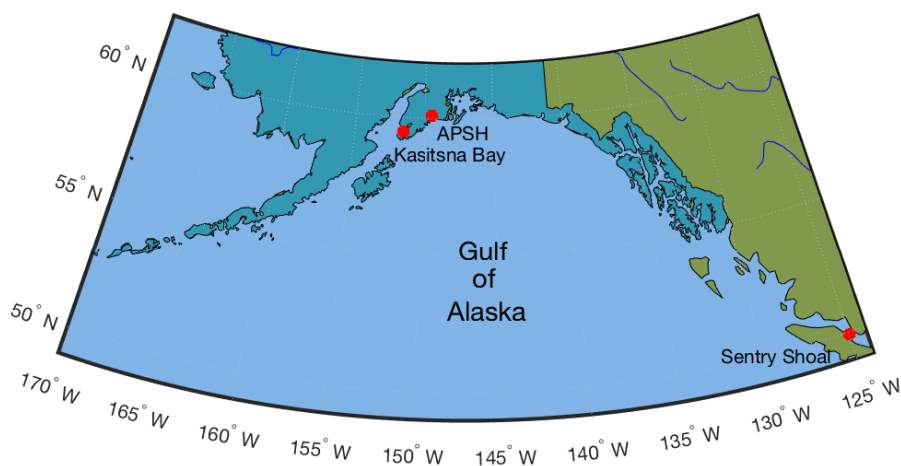


Table 2. One-way Analysis of variance comparing the pH_t error ($\text{SeaFET}^{\text{TM}} \text{pH}_t - \text{BoL } \text{pH}_t$) across calibration methods for both the internal and external electrodes onboard $\text{SeaFETs}^{\text{TM}}_{268}$ at Sentry Shoal (factory calibration and *in situ* single-point calibration) and $\text{SeaFET}^{\text{TM}}_{397}$ at the Alutiiq Pride Shellfish Hatchery (factory calibration, *in situ* single-point calibration, and *in situ* multi-point calibration). Bold type denotes statistical significance.

Site	Electrode	Source	SS	df	MS	<i>F</i>	<i>p</i> -value
APSH	Internal	Fac Cal. Vs. Single-point	27.5	1	27.5	4.96E+04	< 0.001
		Error	0.225	406	0.001		
		Total	27.7	407			
APSH	External	Fac Cal. Vs. Single-point	0.681	1	0.681	536	< 0.001
		Error	0.516	406	0.001		
		Total	1.19	407			
APSH	Internal	Factory Cal. vs. Multi-point	28.3	1	28.3	6.19E+04	< 0.001
		Error	0.185	406	0.001		
		Total	28.5	407			
APSH	External	Factory Cal. vs. Multi-point	0.692	1	0.692	539	< 0.001
		Error	0.521	406	0.001		
		Total	1.21	407			
APSH	Internal	Single-point vs. Multi-point	0.005	1	0.005	15.0	< 0.001
		Error	0.143	406	0.000		
		Total	0.148	407			
APSH	External	Single-point vs. Multi-point	0.000	1	0.000	0.040	0.843
		Error	0.415	406	0.001		
		Total	0.415	407			



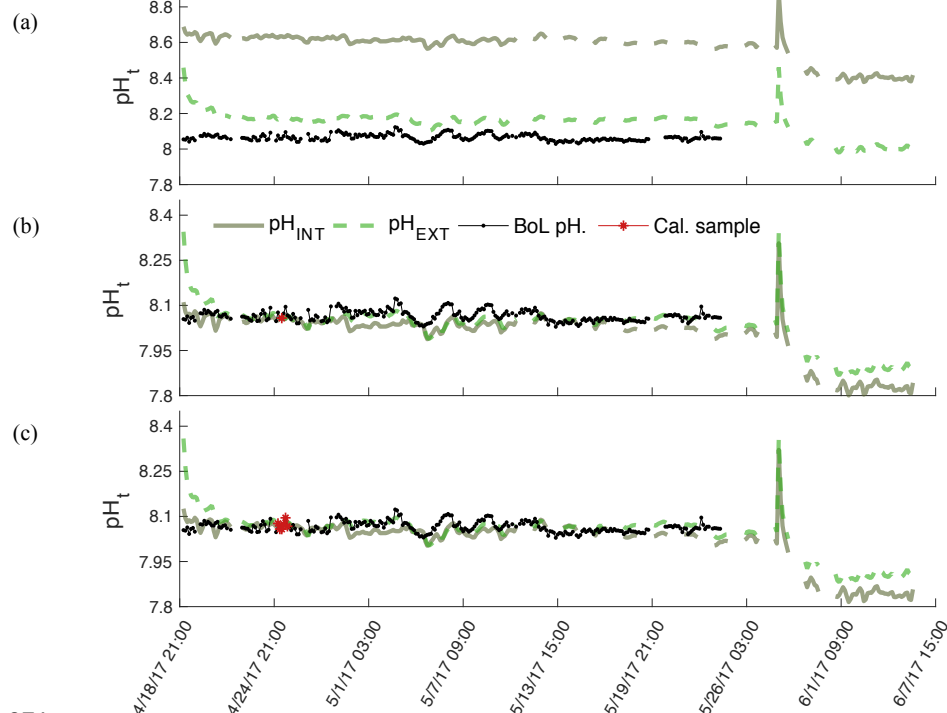
Figure 1.



Geographical map with locations of SeaFETTM field deployments along Alaska's, USA, south-central coast and one location in the Strait of Georgia, British Columbia, Canada.



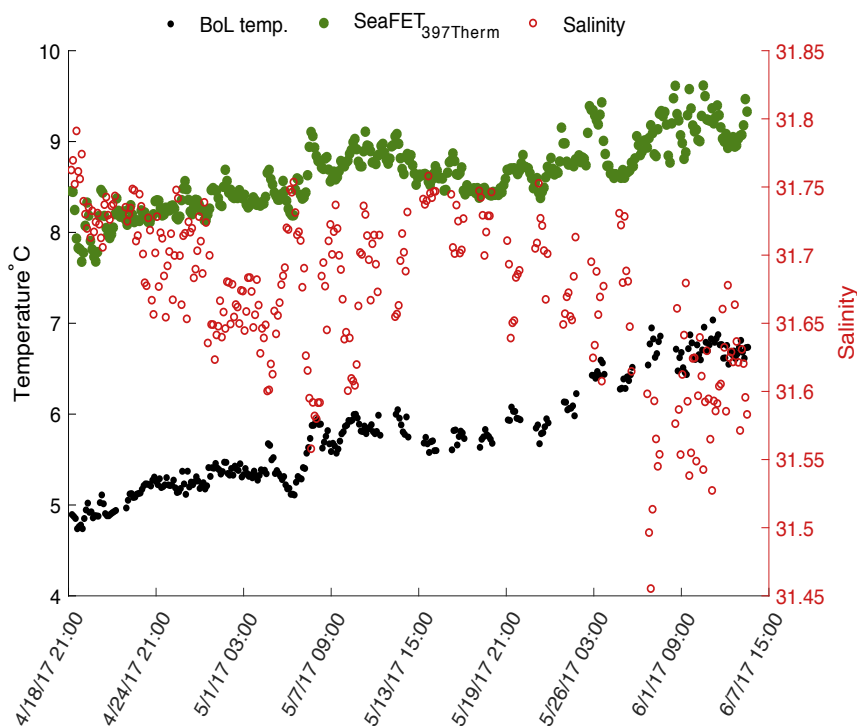
Figure 2.



pH_t recorded by the internal (solid) and external (dashed) electrodes on SeaFETTM₃₉₇ deployed in parallel with the BoL at the Alutiiq Pride Shellfish Hatchery. pH_t from both electrodes is shown when derived using factory calibration (FC) coefficients (panel a), *in situ* single-point (SC) calibration coefficients (panel b), and *in situ* multi-point (MC) calibration coefficients (panel c). Black solid line is pH_t derived from continuous pCO_2 measurements recorded by the BoL and derived TA from the TA-S relationship (Evans et al. 2015). Red circles are the calibration points from the BoL data.



993 **Figure 3.**
 994

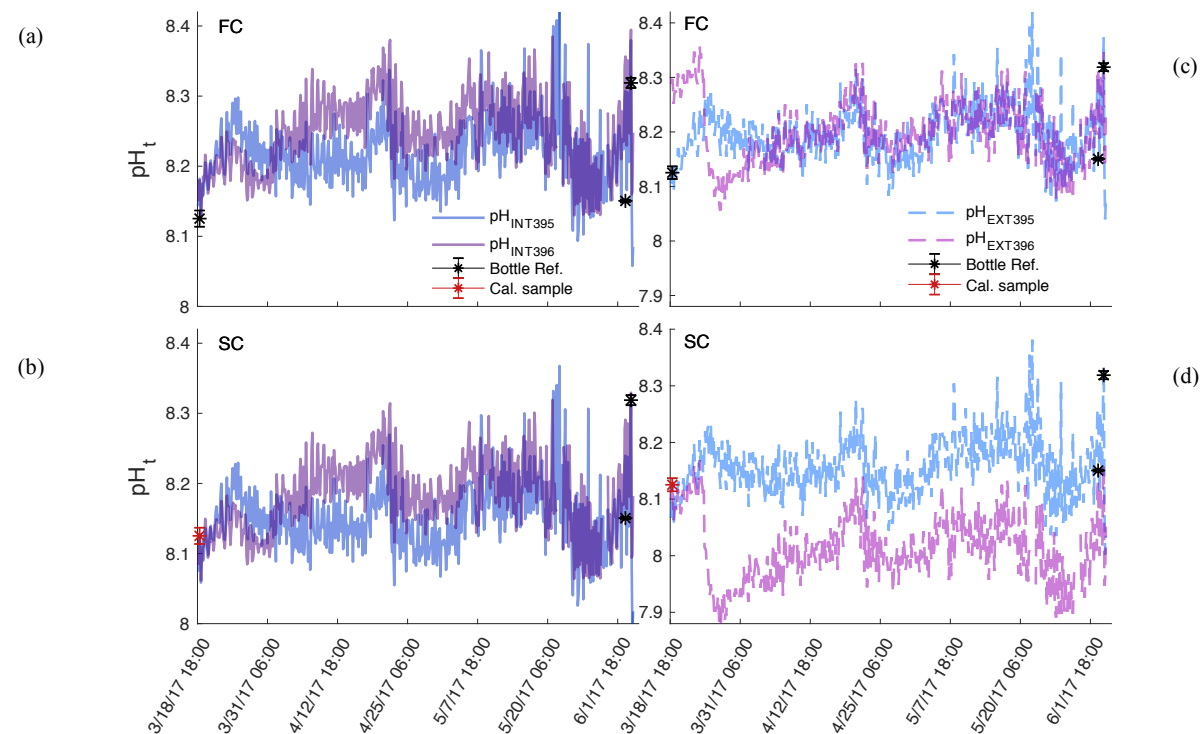


995
 996
 997 Temperature derived from the internal thermistor on SeaFETTM₃₉₇ (green circles) and the
 998 temperature recorded by the BoL (black circles) at the Alutiiq Pride Shellfish Hatchery from late
 999 winter through spring 2017. Salinity (red circles) recorded by the BoL on the right y-axis.

1000
 1001
 1002
 1003
 1004
 1005
 1006
 1007
 1008
 1009
 1010
 1011
 1012
 1013
 1014
 1015
 1016



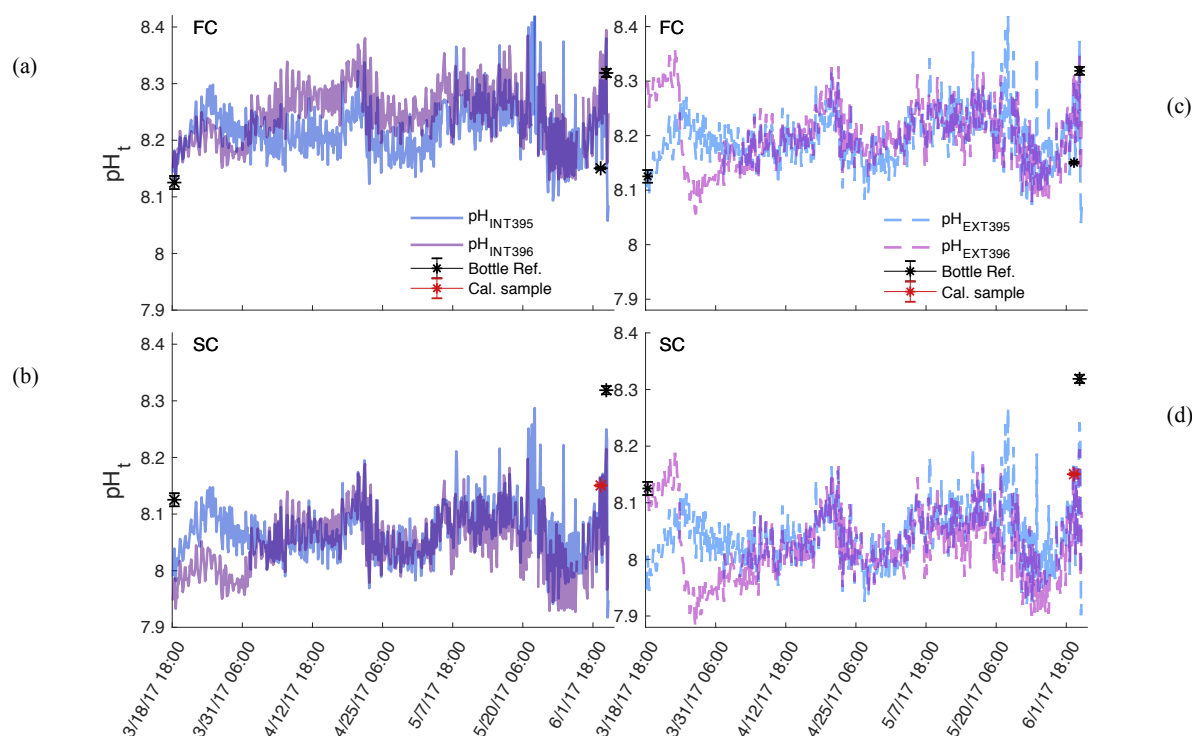
1017 **Figure 4.**
1018



1019
1020
1021 Comparison of pH_t recorded by the internal (panel a and b) and external (panel c and d)
1022 electrodes on SeaFETTM₃₉₅ (blue) and SeaFETTM₃₉₆ (purple) before they were conditioned to the
1023 environment (non-conditioned) deployed in Kasitsna Bay, AK, based on calibration method:
1024 factory calibration (FC) and *in situ* single-point (SC) calibration. Discrete reference samples
1025 (black asterisks) and calibration sample (red asterisks) were collected 36 and 12 h pre-SeaFETTM
1026 recovery, and < 24 h post-deployment, respectively. Temperature and salinity measurements
1027 collected on reference and calibration samples were used to derive SeaFETTM pH_t at those given
1028 time points. All other SeaFETTM pH_t measurements use thermistor temperature and salinity
1029 logged by Kasitsna Bay data sonde.



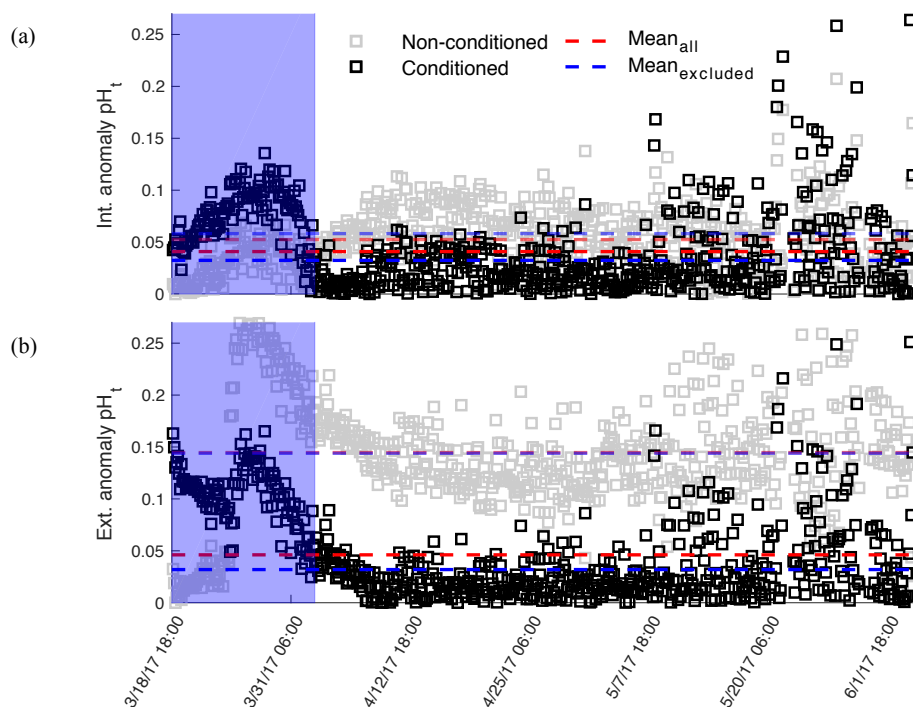
Figure 5.



Comparison of pH_t recorded by the internal (panel a and b) and external (panel c and d) electrodes on conditioned SeaFETTM₃₉₅ (blue) and SeaFETTM₃₉₆ (purple) deployed in Kasitsna Bay, AK, based on calibration method: factory calibration (FC) and *in situ* single-point (SC) calibration. Discrete reference samples (black asterisks) and calibration sample (red asterisks) were collected < 24 h post deployment and 12 h pre-SeaFETTM recovery, while calibration sample was collected 36 h pre-SeaFETTM recovery. Temperature and salinity measurements collected on reference and calibration samples were used to derive SeaFETTM pH_t at those given time points. All other SeaFETTM pH_t measurements use thermistor temperature and salinity logged by Kasitsna Bay data sonde.



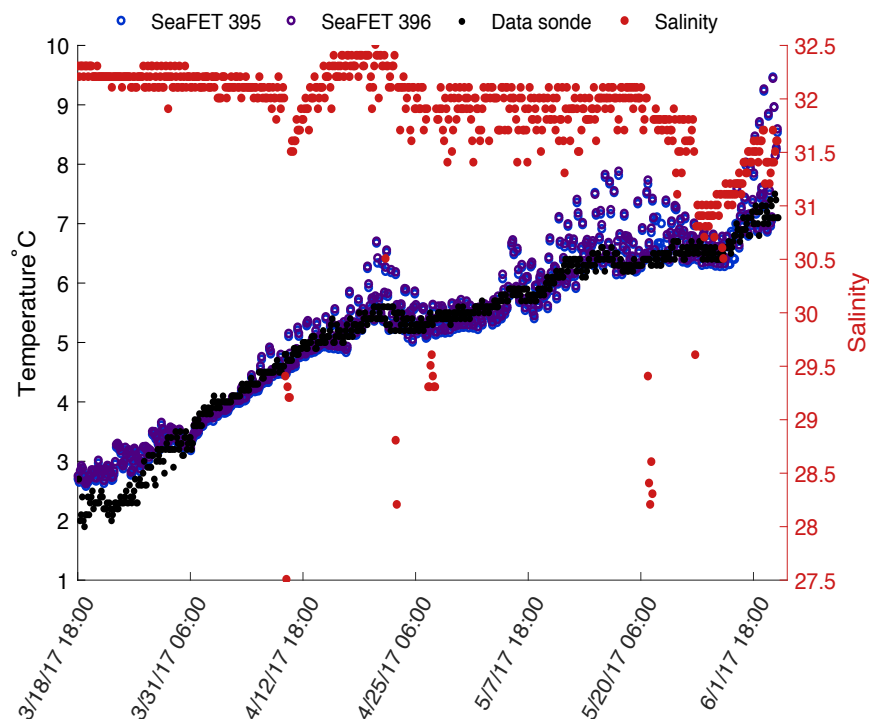
Figure 6.



Mean pH_t anomaly between *in situ* single-point calibrated SeaFETTM₃₉₅ and SeaFETTM₃₉₆ internal (panel a) and external (panel b) electrodes during parallel deployment in Kasitsna Bay, AK. Intra-anomaly comparison based on calibration sample taken at initial deployment (< 24 h non-conditioned, gray squares) and end of deployment (36 h pre-recovery, black squares). Shaded blue region indicates conditioning period. Data points in blue region omitted when mean anomaly was calculated (non-conditioned: transparent blue-dashed line; conditioned: bold blue-dashed line) compared to mean anomaly from entire data set (non-conditioned to environment: red-dashed line; conditioned: red- dashed line).



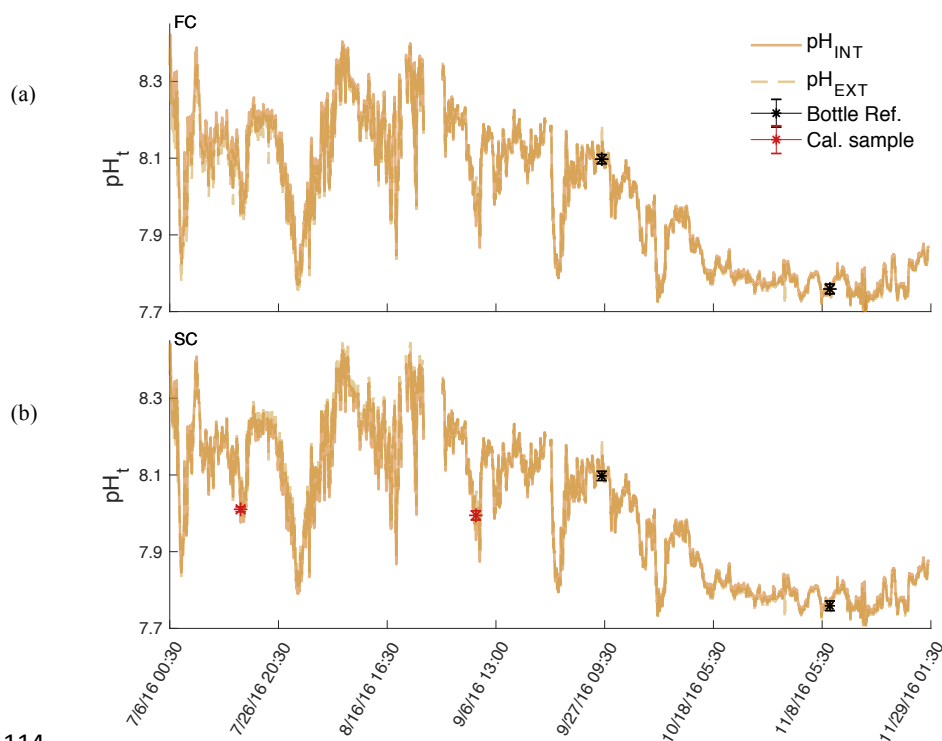
Figure 7.



Temperature derived from the internal thermistor on SeaFETTM₃₉₅ (blue) and SeaFETTM₃₉₆ (purple) compared against the temperature recorded by the Kachemak Bay National Estuarine Research Reserve data sonde. Salinity (Red circles) recorded by Kachemak Bay data sonde on the right y-axis.



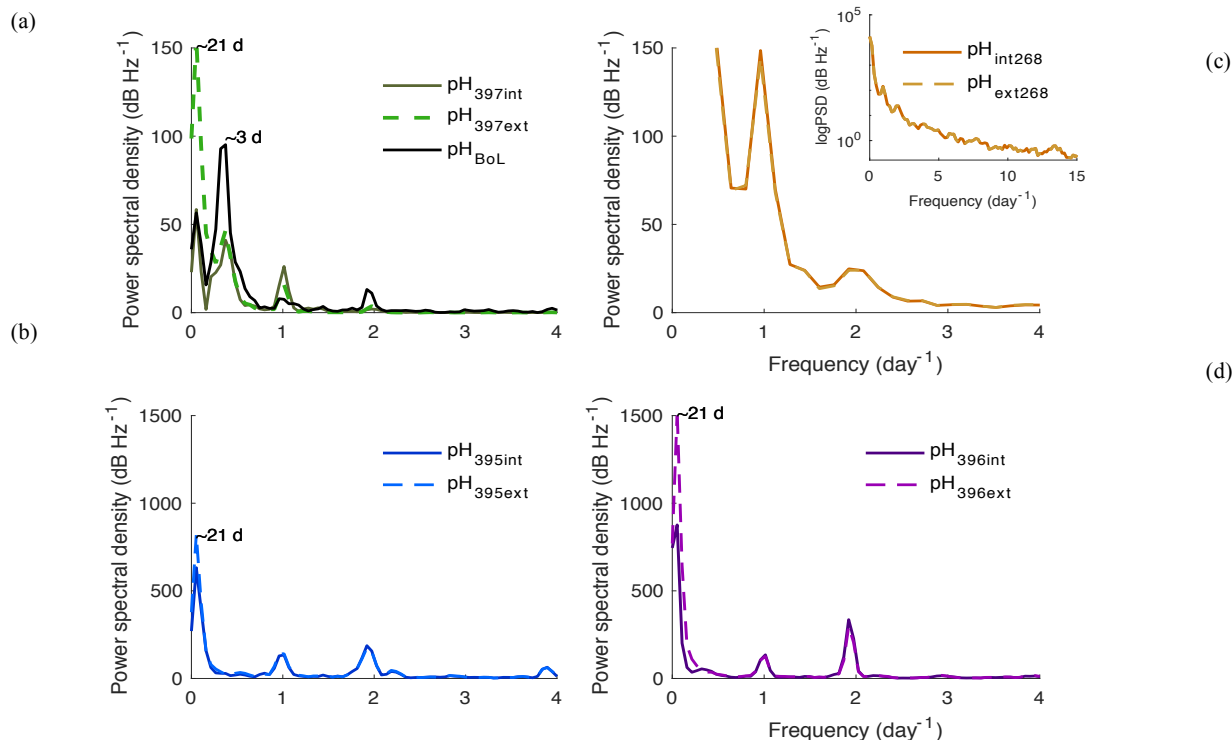
Figure 8.



pH_t recorded by the internal (solid) and external (dashed) electrodes on SeaFETTM₂₆₈ deployed at the Sentry Shoal mooring. pH_t from both electrodes is shown when derived using factory calibration (FC) coefficients (panel a) and *in situ* single-point (SC) calibration coefficients (panel b). Black asterisks are references samples taken after initial calibration and recalibration (red asterisk), where pH_t was derived from TCO_2 and pCO_2 measurements made on the BoL at the Hakai Institute's Quadra Island Field Station.



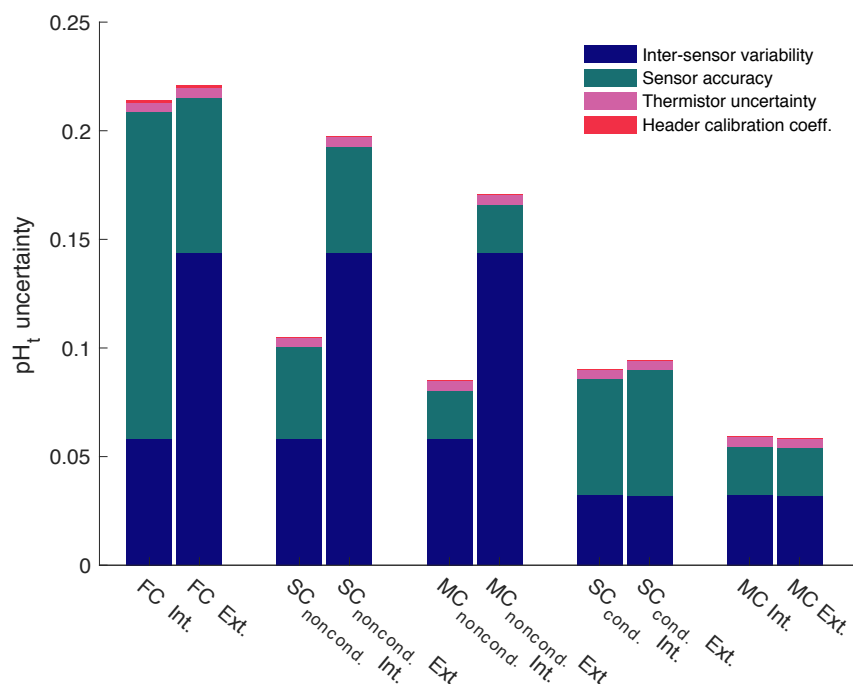
Figure 9.



Power spectral density (PSD) analysis of pH_t in frequency per day for SeaFETs™ 397 (panel a), 268 (panel b), 395 (panel c), and 396 (panel c). Inset in panel b is log base 10 transformed PSD analysis of same data set. All internal electrodes marked as solid colored lines while external electrodes are colored dashed lines. BoL data set marked as solid black line (panel a).



Figure 10



Quantified uncertainties based on field deployments of all Sea-Bird SeaFETs™ separated by electrode calibration method (FC: factory; SC: single-point; MC: multi-point), and calibration time for SeaFETs™ 395 and 396 (i.e., non-conditioned to environment and conditioned). pH_t accuracy uncertainty calculated as the mean difference when comparing the absolute difference between reference samples and SeaFETs™ 395 (non-conditioned to environment and conditioned), 396 (non-conditioned to environment and conditioned), and 268 as well as the average absolute difference between SeaFET™ 397 and the BoL. Inter-sensor variability uncertainty determined by comparing SeaFETs™ 395 (non-conditioned to environment and conditioned) and 396 (non-conditioned to environment and conditioned), deployed side-by-side in Kasitsna Bay. Thermistor uncertainty is calculated pH_t error when using thermistor derived temperature rather than external temperature sensor determined from SeaFETs™ 395 and 396. Header calibration coefficient uncertainty is the discrepancy in pH_t when using SeaFETcom factory calibration coefficients from header file rather than disc file.